

# Necessary Conditions for Tropical Cyclone Rapid Intensification as Derived from 11 Years of TRMM Data

HAIYAN JIANG

*Department of Earth and Environment, Florida International University, Miami, Florida*

ELLEN M. RAMIREZ

*Department of Atmospheric Sciences, University of Utah, Salt Lake City, Utah*

(Manuscript received 12 July 2012, in final form 14 February 2013)

## ABSTRACT

Rainfall and convective properties of tropical cyclones (TCs) are statistically quantified for different TC intensity change categories by using Tropical Rainfall Measuring Mission (TRMM) data from December 1997 to December 2008. Four 24-h future intensity change categories are defined: rapidly intensifying (RI), slowly intensifying, neutral, and weakening. It is found that RI storms always have a larger raining area and total volumetric rain in the inner core. The maximum convective intensity in the inner core is not necessarily more intense prior to undergoing an RI episode than a slowly intensifying, neutral, or weakening episode. Instead, a minimum threshold of raining area, total volumetric rain, and convective intensity in the inner core is determined from the RI cases examined in this study. The following necessary conditions for RI are found in the inner core: total raining area  $> 3000 \text{ km}^2$ , total volumetric rain  $> 5000 \text{ mm h}^{-1} \text{ km}^2$ , maximum near-surface radar reflectivity  $> 40 \text{ dBZ}$ , maximum 20-dBZ (40 dBZ) echo height  $> 8$  (4) km, minimum 85-GHz polarization-corrected brightness temperature (PCT)  $< 235 \text{ K}$ , and minimum 10.8- $\mu\text{m}$  brightness temperature  $< 220 \text{ K}$ . To the extent that these thresholds represent all RI cases, they should be of value to forecasters for ruling out RI. This study finds that total lightning activities in the inner core (outer rainband) have a negative (positive) relationship with storm intensification.

## 1. Introduction

Understanding and predicting intensity changes, especially rapid intensification, of tropical cyclones (TCs) require some understanding of not only the large-scale environment conditions but also the internal dynamical processes. Detailed observations of a storm's internal dynamical field are relatively rarely documented because of the difficulty in measuring the three-dimensional wind fields. On the other hand, there are abundant satellite observations available on the convective and precipitation properties, which, in turn, are influenced by large-scale processes such as environmental interactions and ocean surface fluxes. It has been well established that the necessary environmental conditions of TC intensification and rapid

intensification include warmer sea surface temperatures, higher low- to midtroposphere moisture, and lower vertical wind shear (Merrill 1988; Kaplan et al. 2010). However, Hendricks et al. (2010) found that the rapidly intensifying (RI) and slowly intensifying (SI) cases tend to happen in similar favorable environment conditions. Therefore, they argued that RI is more likely controlled by TC internal processes. Important internal dynamic processes for TC development include spiral rainband dynamics, asymmetric deep convection, eye/eyewall mixing, and eyewall replacement cycles (Hendricks 2012). The vertical motion associated with these horizontally small-scale processes has a convection and precipitation signature in the inner core (IC) and rainband regions. So the quantification of convection and precipitation properties in TCs can provide very useful and perhaps crucial diagnostic information for understanding storm intensity variation.

Convective and precipitation properties in the inner core are closely related to the latent heating release that drives storm development. Previous observational

---

*Corresponding author address:* Dr. Haiyan Jiang, Department of Earth and Environment, Florida International University, 11200 SW 8th Street, PC-342B, Miami, FL 33199.  
E-mail: haiyan.jiang@fiu.edu

studies have shown some relationships between TC intensification and inner core rainfall and convective properties such as rain rate (Rao and MacArthur 1994), convective bursts (Steranka et al. 1986), ice scattering signatures (Cecil and Zipser 1999), hot towers (Kelley et al. 2004, 2005), and lightning activities (Lyons and Keen 1994; Molinari et al. 1999). Many theoretical studies have shown that a TC intensifies as the symmetric overturning circulation draws air from outer radii above the boundary layer while conserving absolute angular momentum (Ooyama 1969; Smith 1981; Shapiro and Willoughby 1982). However, Montgomery and Smith (2011) recently proposed that asymmetric convection/heating was the preferred spinup mechanism. Their argument was based on previous modeling studies recognizing the importance of “vortical hot towers” (VHTs) in the inner core to TC intensification (Hendricks et al. 2004; Montgomery et al. 2006; Nguyen et al. 2008). VHTs are also often referred to as rotating deep convection. It is argued that this local vorticity-rich deep convection plays a very important role in TC intensification through interacting with the parent vortex as the parent vortex intensifies. Although numerical model simulations have shown evidence of VHTs throughout the whole TC intensification process from depression stage all the way to major hurricane stage, including RI periods (e.g., Nguyen et al. 2008), observational evidence of VHTs is mainly reported in the very early stages (mainly depression) of TC development (e.g., Reasor et al. 2005; Sippel et al. 2006; Houze et al. 2009; Bell and Montgomery 2010). Extending the earlier work on two-dimensional and quasi-steady symmetric intensification, Nolan and Grasso (2003) and Nolan et al. (2007) used a three-dimensional framework to show the non-hydrostatic unsteady symmetric response of the tropical cyclone-like vortex to the evolving asymmetries. They found that the symmetric response to the asymmetric motions was much smaller than the symmetric response to the azimuthally averaged heating. This suggests that asymmetric intense convection cells (e.g., hot towers) do not play any specific role in intensification other than to the extent to which they add to the symmetric mean heating.

Fewer studies are documented with a focus on RI. It is still not clear whether the symmetric heating or asymmetric heating is more important to RI. Jiang (2012) compared the satellite-observed convective properties [i.e., radar reflectivity profiles, infrared (IR) cloud-top temperature, and passive microwave ice scattering signature] in the inner core for 24-h future rapidly intensifying, slowly intensifying, neutral (N), slowly weakening, and rapidly weakening storms. To partially test the

VHT theory, the hypothesis of Jiang (2012) was that the existence of hot towers (defined as maximum 20-dBZ echo height  $\geq 14.5$ -km radar) in the inner core is the sufficient condition for RI. Jiang found that both the probability of RI and the probability of slowly intensifying increase, and both the probability of slowly weakening and probability of rapidly weakening decrease for samples with hot towers in the inner core. However, the increases in probabilities for intensifying and decreases for weakening are not substantial. Therefore, Jiang (2012) argued that hot towers are neither necessary nor a sufficient condition for RI. The analysis of Jiang (2012) RI focused on convective intensity properties in the inner core, especially on hot towers.

Kieper and Jiang (2012) demonstrated that a precipitative ring pattern around the TC center is a very good predictor of RI. The ring was seen from the 37-GHz passive microwave observations for numerous TCs that were undergoing RI. From simultaneous radar vertical cross sections, the inner edge portion of the ring is nearly 100% closed surrounding the TC center and mainly consists of shallow precipitation from near or below the freezing level to the surface. The outer edge portion of the ring could have asymmetric intense convection (i.e., hot towers) embedded within the ring. This outer edge portion of intense convection is highly asymmetric. The results of Kieper and Jiang (2012) strongly support the theory that the symmetric heating is more efficient at spinning up a cyclone than asymmetric heating. Kieper and Jiang (2012) suggest that a particular condition that is necessary for RI is widespread precipitation with high total volumetric precipitation in the inner core. They demonstrated that the ring and favorable environment condition together could be the nearly sufficient condition for RI. However, their study focused on the predictive power of the ring pattern. No quantitative analysis was documented for the threshold of the particular inner core necessary condition for RI. The first purpose of this study is to quantitatively demonstrate that the large raining area and high total volumetric rain in the inner core is a necessary condition for RI. Moderate convective intensity will be demonstrated to occur simultaneously under this condition. Using 11 years of Tropical Rainfall Measuring Mission (TRMM) satellite data, a set of minimum values in terms of rainfall and convective properties will be determined in order to describe this particular necessary condition for RI. Directly applicable to radar and satellite observational data, these minimum values will provide a simple and useful tool for forecasters to rule out RI. Like the well-accepted 26°C sea surface temperatures necessary for TC formation, in this paper

we search for a necessary RI condition,<sup>1</sup> which could have very useful forecasting applications.

DeMaria et al. (2012) examined the relationships between lightning activity and RI using 6 years of World Wide Lightning Location Network (WWLLN) data for TCs in the Atlantic and eastern North Pacific Oceans. Surprisingly, they found that rapidly weakening TCs have larger lightning density in the inner core (0–100 km) than RI storms, and the lightning density in the rainband regions (200–300 km) is higher for storms that rapidly intensified in the following 24 h. However, as indicated by DeMaria et al. (2012), the fixed radius distance used in their study caused some structure loss, especially when studying a large sample of TCs with various storm sizes (e.g., Atlantic versus northwestern Pacific storms). A question resulting from this data is whether their results hold true when using a more appropriate method to separate inner core and rainband regions. The second purpose of this study is to study the relationship between lightning and RI for different TC regions.

Jiang et al. (2013, hereafter JRC) document the distributions of convective and rainfall properties in TC inner cores and rainbands in the dataset used here. To account for varying TC sizes, JRC manually separated inner core, inner rainband (IB), and outer rainband (OB) regions for all the TRMM satellite TC overpasses from December 1997 through December 2008. The separation is based on convective structure, such as the horizontal fields of radar reflectivity and passive microwave ice scattering. In this study, particular TRMM-derived rainfall and convective parameters to be examined include raining area, rain rate, total volumetric rain, radar reflectivity, passive microwave brightness temperature at 85 and 37 GHz, IR cloud-top brightness temperature, and lightning flash counts. The organization of the remainder of the paper is as follows. The data and methodology are briefly described in section 2. The distributions of these rainfall and convective properties as a function of different TC intensity change categories are presented in section 3. A series of necessary conditions for RI in terms of these inner core properties are also presented in section 3. Discussions are provided in section 4 and conclusions in section 5.

## 2. Data and methodology

### a. TRMM TC data

The same dataset from the TRMM Tropical Cyclone Precipitation Feature (TCPF) database (Jiang et al. 2011) is used in this study as in JRC. It includes global TCs that were observed by the TRMM satellite from December 1997 through December 2008. The categorization of IC, IB, and OB regions in TRMM TC overpasses is described in section 2a of JRC. As in JRC, two sets of samples are used in this study in order to maximize the sample size and use the unique three-dimensional observations from the radar: one is from TRMM overpasses within the TRMM Microwave Imager (TMI) swath, and the other is within the Precipitation Radar (PR) swath. The selection of TRMM overpasses is described in section 2c of JRC. In this study, TRMM-derived parameters selected for the analysis of TC samples in the TMI swath include minimum 85-/37-GHz polarization-corrected brightness temperatures (PCTs; Spencer et al. 1989; Cecil et al. 2002); minimum 11- $\mu\text{m}$  brightness temperature  $T_{\text{B11}}$ ; percentage of pixels with 85-GHz PCT less than 250 and 225 K; 2A12 (Kummerow et al. 1996) conditionally mean rain rate, raining area, and total volumetric rain; and lightning flash counts. The term  $T_{\text{B11}}$  is observed by the TRMM Visible and Infrared Scanner (VIRS), and lightning flash counts are observed by the Lightning Imaging Sensor (LIS) on TRMM. All other parameters are observed by the TMI. The swath widths of VIRS and LIS are similar to that of TMI, while the PR has a much narrower swath. Parameters selected for the analysis of samples in the PR swath include a vertical profile of maximum radar reflectivity; maximum near-surface reflectivity; maximum height of 20-, 30-, and 40-dBZ radar echo; and 2A25 (Iguchi et al. 2000) conditionally mean rain rate, raining area, and total volumetric rain. All these parameters are observed by the PR. Section 2d of JRC provided a review of the physical meanings of these parameters and how they are referred to as convective and rainfall proxies.

JRC compared the convective and rainfall properties among IC, IB, and OB regions in terms of large precipitation features. However, in this study each TRMM overpass (i.e., each storm) is assigned a single value of rainfall and convective parameters for IC, IB, and OB regions, respectively. Since multiple features usually exist in the IC, IB, or OB region of one TC, we consider this storm-based approach to be more appropriate for studying TC intensity changes. The number of TMI (PR) TC overpasses used in this study is 2712 (1100). The geographic distributions of these overpasses are given in Fig. 1. For parameters other than lightning

---

<sup>1</sup> It would be ideal to search for both necessary and sufficient conditions. However, results from this study and other previous studies indicate that no sufficient condition exists for RI in terms of the storm convective and rainfall properties only. It is possible to find some “nearly sufficient condition” if combining both environmental and storm internal parameters, which is beyond the topic of this study.

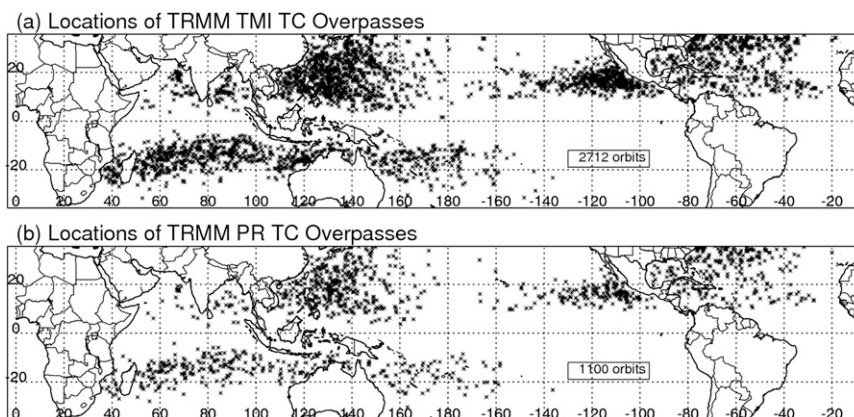


FIG. 1. Locations of TRMM (a) TMI and (b) PR swath TC overpasses used in this study. The number of orbits is provided within the panels.

flashes, only the inner core region is examined for the relationships with TC intensity changes. For lightning activities, both inner and rainbands are investigated to compare with the results of DeMaria et al. (2012).

#### b. Selection of TC intensity change categories

The TCPF database includes all intensity stages of TCs that reached tropical storm intensity level or above at least once in their lifetime. Therefore, each individual TRMM overpass included here could be at tropical depression, tropical storm, or hurricane stage. The 24-h future storm intensity and intensity change corresponding to each overpass are interpolated from the 6-h best-track data from the National Hurricane Center (NHC) for TCs in the North Atlantic and eastern North Pacific basins and from the Joint Typhoon Warning Center (JTWC) for TCs in other basins. The TMI and PR swath samples are separated into four intensity change categories: RI, SI, N, and weakening (W). Table 1 lists the four intensity change categories, along with the range and sample size. The threshold for each category is defined by following Jiang (2012).

Table 2 shows the distribution of the different intensity change samples as a function of the initial TC

intensity. For both TMI and PR swath samples, storms that are initially of tropical storm intensity account for the largest percentage of RI cases while category 1–2 hurricanes contribute the next largest percentage. Generally, the RI probability for tropical storms is greater than that of hurricanes. Both tropical depressions and tropical storms account for a larger percentage of slowly intensifying cases, while category 1–2 hurricanes account for most of the weakening cases. In terms of different TC-prone basins (Table 3), RI cases are found most in the northwestern Pacific and least in the northern Indian Ocean. Note that the distribution as a function of different basins is similar for different intensity change categories.

### 3. Results

#### a. Rainfall

Figure 2 shows the cumulative distribution functions (CDFs) of TMI 2A12 (Kummerow et al. 1996) and PR 2A25 (Iguchi et al. 2000) raining area, volumetric rain, and conditionally mean rain rate in the inner core region for different intensity change storms. Significance tests using the unequal variance *t*-test method have been

TABLE 1. Definition of RI, SI, N, and W intensity change categories and respective TMI- and PR-observed TC overpasses. The terms  $v_{\max}$  and  $v_{\max24}$  are the current (at the TRMM observation time) and future 24-h maximum wind speed intensity of the storm.

Category	Max wind speed range (kt)	TC overpasses	
		TMI	PR
RI	$v_{\max24} - v_{\max} \geq 30$	181	64
SI	$10 \leq v_{\max24} - v_{\max} < 30$	779	316
N	$-10 < v_{\max24} - v_{\max} < 10$	1183	490
W	$v_{\max24} - v_{\max} \leq -10$	569	230
Total		2712	1100

TABLE 2. The distribution of different intensity change samples as a function of different initial TC intensities [i.e., tropical depression (TD), tropical storm (TS), category 1–2 (CAT12) and 3–5 (CAT35) hurricanes] for TMI and PR swath samples.

Category	TMI swath				PR swath			
	TD	TS	CAT12	CAT35	TD	TS	CAT12	CAT35
RI	31	83	63	4	9	32	21	2
SI	312	306	114	47	127	120	48	21
N	502	395	184	102	200	166	86	38
W	8	188	215	158	4	73	87	66

TABLE 3. The distribution of different intensity change samples as a function of different TC basins [i.e., Atlantic Ocean (ATL), eastern central Pacific Ocean (EPA), northwestern Pacific Ocean (NWP), northern Indian Ocean (NIO), southern Indian Ocean (SIO), and South Pacific Ocean (SPA)] for TMI and PR swath samples.

Category	TMI swath						PR swath					
	ATL	EPA	NWP	NIO	SIO	SPA	ATL	EPA	NWP	NIO	SIO	SPA
RI	26	23	72	7	3	15	11	6	30	0	12	5
SI	137	91	291	36	160	64	65	33	121	16	50	31
N	239	211	322	53	276	82	114	77	134	16	122	27
W	96	127	166	15	113	52	40	53	71	5	40	21

done to test the differences of these rainfall parameters for RI versus other intensity change groups. The results show that the differences for raining area and volumetric rain are statistically significant at the 99.99% level, while the differences for rain rate are statistically significant at the 95% level. From Fig. 2, it is obvious that storms that will undergo RI always have larger raining area and total volumetric rain in the inner core region than storms that will slowly intensify, be neutral, or weaken. Note that the  $x$  axes of Figs. 2a, 2b, 2d, and 2e are in log scale; therefore the difference is large even for small spacing among the curves. From Fig. 2, it is also interesting to observe that the minimum values (when the CDFs

start to become greater than 0%) of raining area and volumetric rain for RI storms are much larger than those corresponding minimum values for storms in other intensity change categories. For example, the minimum value of inner core 2A12 and 2A25 raining area (volumetric rain) is about 3000 km<sup>2</sup> (5000 mm h<sup>-1</sup> km<sup>2</sup>) for RI storms, but only reaches 100 km<sup>2</sup> (100 mm h<sup>-1</sup> km<sup>2</sup>) for storms in other intensity change stages. This quantitatively confirms the finding of Kieper and Jiang (2012) that a particular condition necessary for RI is widespread precipitation with high total volumetric precipitation in the inner core. A minimum threshold of raining area and total volumetric rainfall amount in the

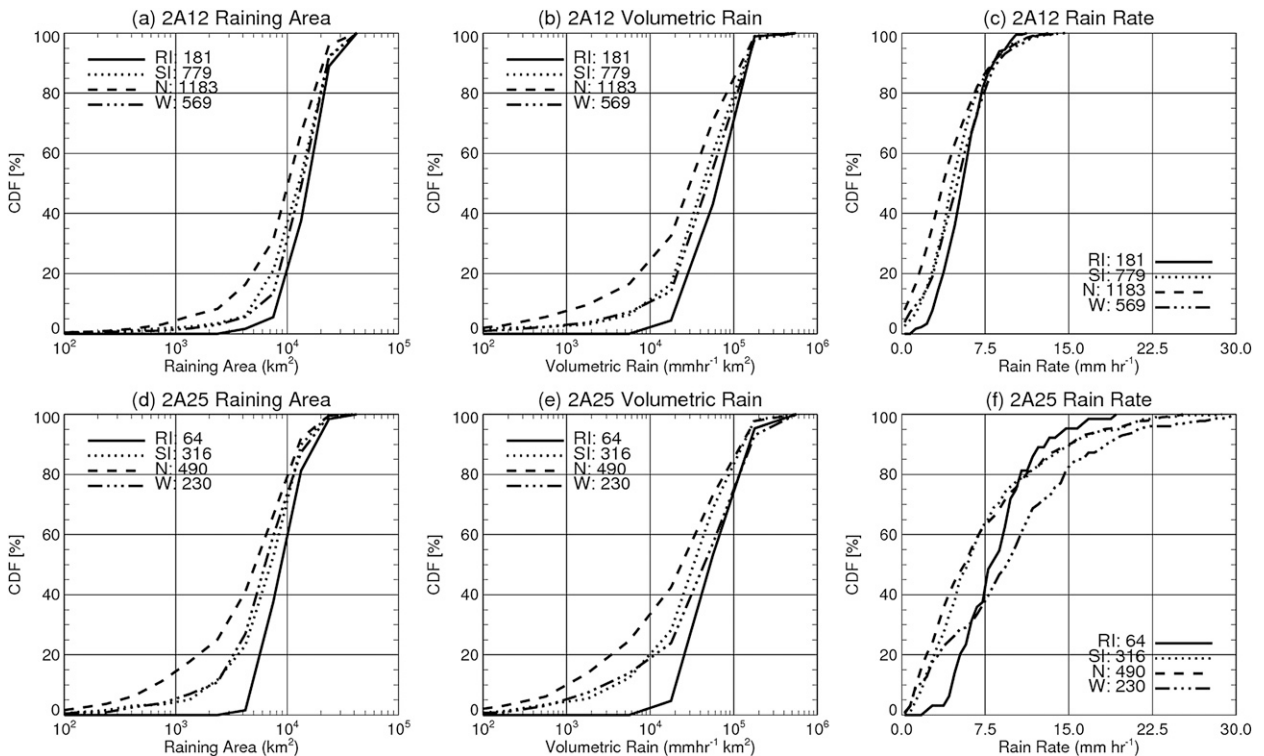


FIG. 2. CDFs of TMI-derived 2A12 (a) raining area, (b) volumetric rain, and (c) conditionally mean rain rate, and PR-derived 2A25 (d) raining area, (e) volumetric rain, and (f) conditionally mean rain rate in the inner core of TCs in different intensity change stages.

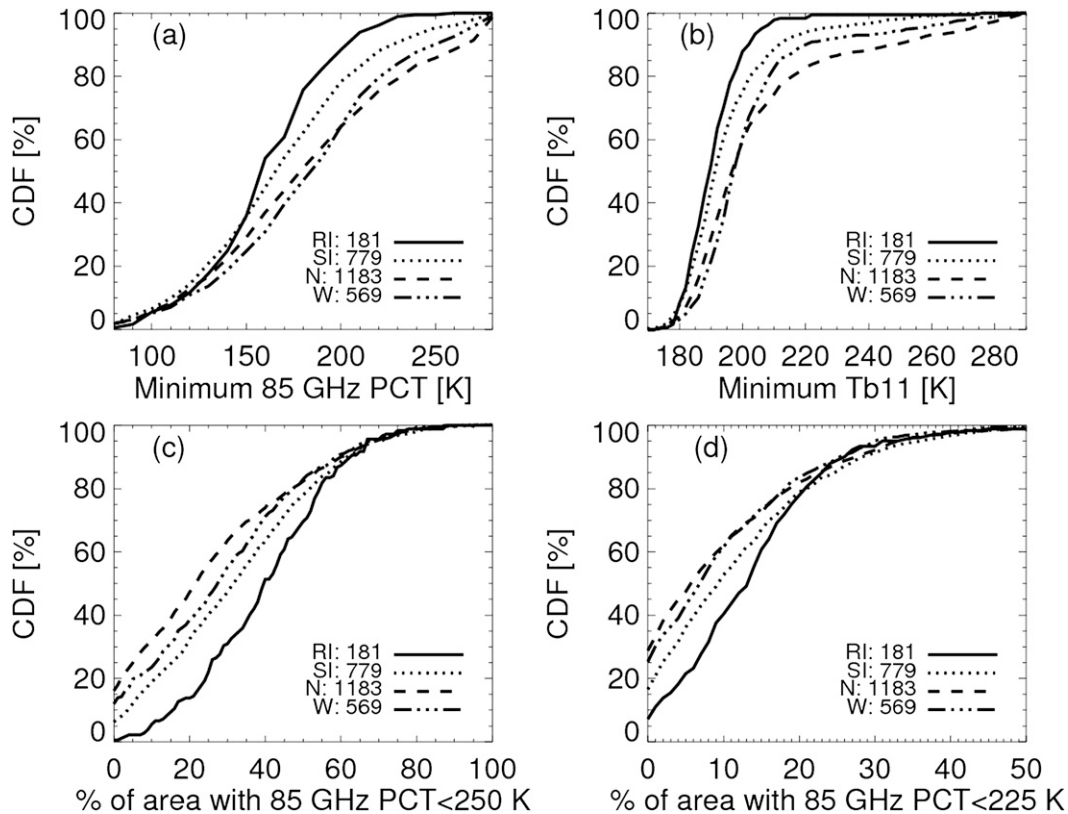


FIG. 3. CDFs of (a) minimum 85-GHz PCT (K), (b) minimum  $T_{B11}$  (K), and percentages of inner area with 85-GHz PCT less than (c) 250 and (d) 225 K in the inner core of TCs in different intensity change stages.

inner core has to be reached before a storm undergoes RI. The necessary conditions for RI found from Fig. 2 include that 1) total raining area in the inner core region is greater than  $3000 \text{ km}^2$  (Figs. 2a,d), and 2) the total volumetric rain in the inner core is greater than  $5000 \text{ mm h}^{-1} \text{ km}^2$  (Figs. 2b,e).

Unlike raining area and volumetric rain, the conditionally mean rain rate in the inner core is an indicator of precipitation intensity. From Figs. 2c and 2f, although in the lower rain-rate spectrum ( $<7.5 \text{ mm h}^{-1}$ ) the CDFs show that RI storms have higher conditionally mean rain rate in the inner core than storm in other intensity change categories, in the higher rain-rate spectrum ( $\geq 9.5 \text{ mm h}^{-1}$ ) RI storms have lower conditionally mean rain rate in the inner core. No necessary conditions for RI in terms of conditionally mean rain rate in the inner core are found. The rainfall and raining area estimates from the TMI 2A12 and PR 2A25 are independent retrievals. It is not surprising that differences exist between TMI-derived 2A12 and PR-derived rainfall retrievals because of the discrepancy inherent within the PR 2A25 and TMI 2A12 algorithms. For example, the PR 2A25 rain rates (Fig. 2f) have much greater values in the high end of the CDF than those in the TMI 2A12 rain rates. However,

similarities between 2A12 and 2A25 raining area and volumetric rain produce the same necessary condition for RI.

#### b. Convective intensity proxies: Brightness temperatures and vertical profiles of radar reflectivity

As described in JRC, low values of 85- and 37-GHz PCT tend to indicate strong ice scattering signatures, and low values of IR  $T_{B11}$  indicate higher cloud tops. Therefore, all these parameters can be used as convective intensity proxies. Significance tests using the unequal variance  $t$ -test method have been done to test the differences of the minimum 37- and 85-GHz PCTs, minimum IR  $T_{B11}$ , and percentages of inner core area with 85-GHz PCT less than 250 and 225 K convective parameters for RI versus other intensity change groups. The results show that the differences for all parameters but the minimum 37-GHz PCT are statistically significant at the 95% level. The CDFs of the minimum 85-GHz PCT, minimum IR  $T_{B11}$ , and percentages of inner core area with 85-GHz PCT less than 250 and 225 K in the inner core for storms in different intensity change stages are presented in Fig. 3. It is seen from Figs. 3a and

3b that at a weaker convective spectrum (i.e., minimum 85-GHz PCT greater than  $\sim 150$  K, minimum 37-GHz PCT greater than  $\sim 250$  K, and minimum  $T_{B11}$  greater than 180–185 K) RI storms have a stronger ice scattering signature and higher cloud top in the inner core than storms in the other three intensity change categories, and slowly intensifying storms show much stronger convective intensity than neutral and weakening storms. However, at the stronger convective spectrum, no significant difference among different intensity change categories is seen in the distributions of these convective parameters. This indicates that RI storms do not necessarily have the strongest convection in the inner core.

Similar to Fig. 2, it is also interesting to observe that the maximum values (when the CDFs reach 100%) of the minimum 85-GHz PCT and IR  $T_{B11}$  for RI storms are much lower than those corresponding maximum values for storms in other intensity change categories. For example, the maximum value of minimum 85-GHz PCT (IR  $T_{B11}$ ) is about 235 K (220 K) for RI storms but reaches 280 K (260–280 K) for storms in other intensity change stages. This indicates that a minimum threshold of convective intensity in the inner core has to be reached before a storm undergoes RI. The minimum convective intensity might be a symptom of the minimum raining area and total volumetric rain condition for RI found in Fig. 2. Whether it is true or not, the necessary convective intensity condition for RI derived from Figs. 3a and 3b are that 1) minimum 85-GHz PCT in the inner core is less than  $\sim 235$  K and 2) minimum IR  $T_{B11}$  in the inner core is less than  $\sim 220$  K. A threshold of 250 K for the 85-GHz PCT is considered an indicator of moderate rain (Spencer et al. 1989; Mohr and Zipser 1996a,b), and 85-GHz PCT less than 225 K has been used as a criterion of convection (McGaughey et al. 1996; Mohr and Zipser 1996a,b). Therefore, the 235 K threshold of minimum 85-GHz PCT found here represents moderate-to-heavy rain. The traditional way to define deep convection from IR measurements is finding pixels with brightness temperatures colder than a given temperature threshold from IR images. This threshold could be 208 K (Mapes and Houze 1993; Hall and Vonder Haar 1999), 210 K (Zuidema 2003), 218 K (Machado et al. 1998), or the cold point tropopause temperature (Gettelman et al. 2002). As shown in Gettelman et al. (2002), the cold point tropopause temperature over the tropics varies between 180 and 206 K. The base of the tropopause region is about 215 K. Therefore, the 220 K of IR  $T_{B11}$  represents convective clouds that are close to, but not as deep as, overshooting convection (i.e., hot towers). Minimum brightness temperatures are extreme values that represent just one pixel in the inner core. The percentage of area satisfying a given PCT

threshold is perhaps a more appropriate convective proxy. Figure 3c indicates that the inner core of RI storms contains a larger percentage of area with 85-GHz PCT less than 250 K (moderate rain), followed by slowly intensifying, weakening, and neutral storms. This is also generally true for the percentage of area with 85-GHz PCT less than 225 K (convection; Fig. 3d).

Vertical profiles of radar reflectivity can also be used as a proxy of convective intensity. Figure 4 shows the contoured frequency by altitude diagrams (CFADs; Yuter and Houze 1995) of maximum radar reflectivity in the inner core of TCs in different intensity change stages. The same *t*-test method used in Fig. 2 has been used here to test the statistical significance of the differences of the maximum reflectivity at each level for RI versus other intensity change groups. The results show that the differences are statistically significant at the 95% level. From Fig. 4, we can see that the distribution is highly concentrated around the median profile for storms that will undergo RI, while a wider distribution is seen for storms in other intensity change categories. From Fig. 5, no significant difference is seen in the top 10% of maximum radar reflectivity profiles among storms in different intensity change categories, except that the weakening storms seem to have stronger reflectivities below the freezing level than RI storms. The main reason is that a large fraction of weakening storms has stronger initial intensity (i.e., 28% major hurricanes and 38% category 1–2 hurricanes; Table 2). As shown in JRC, stronger TCs, especially major hurricanes, have much heavier near-surface rain rate and lower-level reflectivities in the inner core, while extremely strong convection (indicated by strong ice scattering signature and upper-level radar reflectivity) is often seen in tropical storms and depressions. As seen in Table 2, about 46% of RI storms are tropical storms and 17% of them are tropical depressions. The median profile of RI storms shows much higher reflectivities above 10 km than storms in other intensity change categories. The median height of maximum 20-dBZ echo reaches about 14.5 km for RI storms, while this value is only 12.5, 12, and 11 km for slowly intensifying, neutral, and weakening storms, respectively. The biggest difference among different intensity change categories is in the bottom 10% of inner core maximum reflectivity profiles. For RI storms, the bottom 10% of the profile is much stronger than that of other intensity change categories and is almost as strong as the median profiles of neutral and slowly intensifying storms. At near surface, the bottom 10% of maximum reflectivity in the inner core of RI storms is 46 dBZ, which is 8, 12, and 12 dBZ stronger than that of slowly intensifying, neutral, and weakening storms, respectively. The bottom 10% of maximum 20-dBZ echo

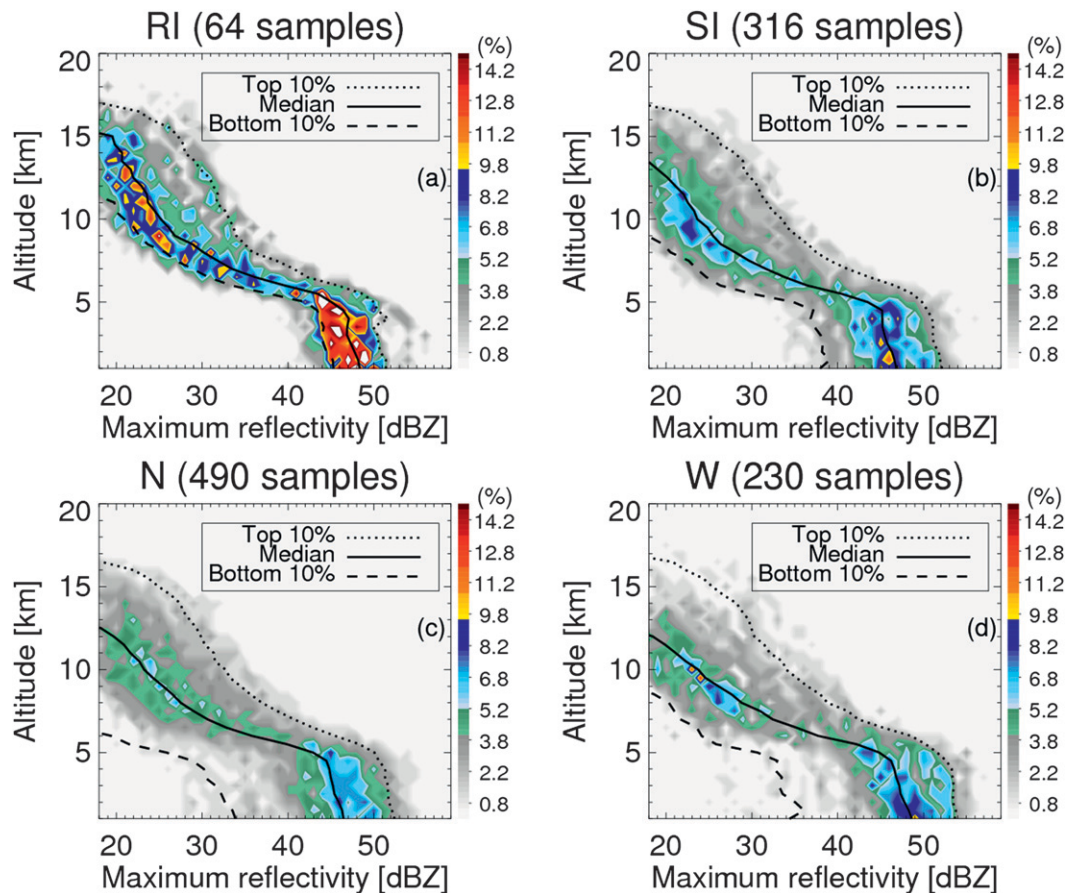


FIG. 4. CFADs of maximum radar reflectivity in the inner core of TCs in (a) RI, (b) SI, (c) N, and (d) W intensity change stages. Bottom 10th percentile (dashed lines), median (solid lines), and 90th percentile (dotted lines) of vertical profiles of maximum radar reflectivity are shown in each panel.

height in the inner core of RI storms is 10 km, which is 2, 2, and 4 km higher than that of slowly intensifying, neutral, and weakening storms, respectively. Just as is discussed above, Figs. 4 and 5 indicate that a necessary condition (i.e., a minimum threshold of convective intensity in the inner core) has to be reached before a storm undergoes RI.

The box and whisker plots in Fig. 6 represent the distributions of maximum near-surface reflectivity, maximum heights of 20- and 40-dBZ radar echo in the inner core. The top of the box represents the 75% percentile, the center line the median, and the bottom of the box the 25% percentile. The whiskers extend out to the maximum or minimum value of the data or to 1.5 times either the 75% or 25% percentile, if there are data beyond this range. Outliers are plotted individually with circles. The same *t*-test method as used in Fig. 2 has been used here to test the statistical significance of the differences of these radar parameters for RI versus other intensity change groups. The results show that the differences are

statistically significant at the 99% level. The distributions in Fig. 6 are much narrower for RI storms than those for storms in other intensity change categories. For RI storms, the maximum near-surface reflectivity in the inner core never goes under 40 dBZ, and the maximum heights of 20- and 40-dBZ radar echo in the inner core never drop lower than 8 and 4 km, respectively. These are the necessary conditions for RI.

### c. Lightning

TRMM observations within the TMI swath (similar swath width to LIS) are used in this section to compare lightning characteristics in the inner core, inner rainband, and outer rainband regions for different intensity change categories. Figure 7a shows the percentage of TRMM TC overpasses with lightning in different TC regions and intensity change categories. For the inner core region with lightning, the percentage is the lowest for storms that will undergo RI and the highest for weakening storms. Only about 7% of RI storms have

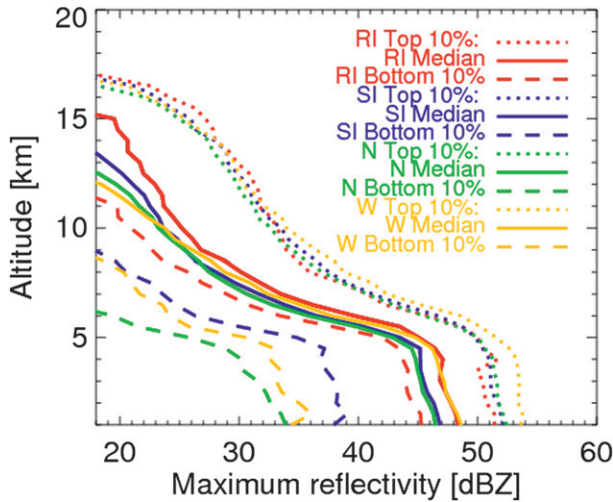


FIG. 5. Bottom 10th percentile (dashed lines), median (solid lines), and 90th percentile (dotted lines) of vertical profiles of maximum radar reflectivity in the inner core of TCs in different intensity change stages.

lightning in the inner core, while the percentage is about 11%–12% for storms in other intensity change categories. For the outer rainband region, the reverse relationship is seen. The percentage of overpasses with lightning in the outer rainband region is the highest for RI storms (37%), followed by storms in slowly intensifying (33%), neutral (25%), and weakening (20%) categories.

Figure 7b shows the flash count per 2A12 raining area for inner core, inner rainband, and outer rainband regions of TCs in different storm intensity categories. After normalizing the flash counts by 2A12 raining area,

lightning production in the inner core region is the lowest for storms that will undergo RI, second lowest for slowly intensifying storms, third lowest for weakening storms, and highest for neutral storms. The lightning density per raining area in the inner core for RI storms is more than a factor of 2 smaller than that for neutral and weakening storms. Generally, it is seen that the lightning density per raining area in the inner core increases as the rate of intensification decreases. In the inner rainband region, the lightning density (per raining area) is the highest for neutral storms and the lowest for weakening storms, with RI and SI categories in between. In the outer rainband region, the order is almost the reverse of the inner core region. The lightning density per raining area in the outer rainband region increases as the rate of intensity change increases. In the outer rainband region, storms that will undergo RI have the highest flash count per raining area, while storms that will weaken have the lowest flash density. Besides raining area, additional parameters, such as the 2A12 volumetric rain, the area of 85-GHz PCT less than 250 K, and the area of 85-GHz PCT less than 225 K, are used to normalize the flash counts. Similar to Fig. 7b, lightning density normalized by these additional parameters in the inner core (outer rainband) decreases (increases) as the rate of storm intensification increases (not shown).

#### 4. Discussions

Results in sections 3a and 3b indicate that RI storms do not necessarily have more extremely intense convection in the inner core than non-RI storms. Instead, a minimum threshold of raining area, total volumetric

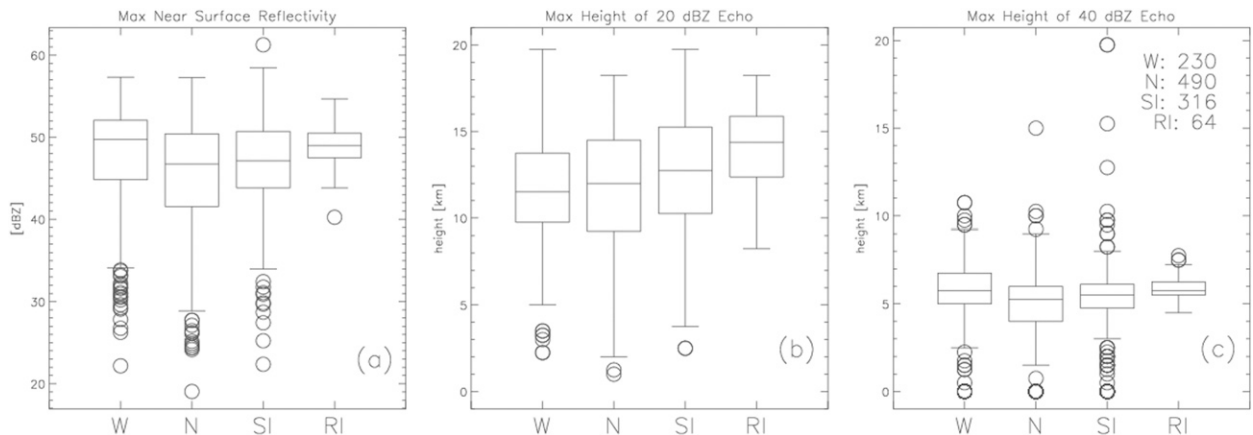


FIG. 6. Box and whisker plots of 2A25 (a) maximum near-surface radar reflectivity, (b) maximum height of 20-dBZ radar echo, and (c) maximum height of 40-dBZ radar echo in the inner core of TCs in different intensity change stages. The top of the box represents the 75th percentile, the center line the median, and the bottom of the box the 25th percentile. The whiskers extend out to the maximum or minimum value of the data or to 1.5 times either the 75% or 25% percentile, if there are data beyond this range. Outliers are plotted individually with circles.

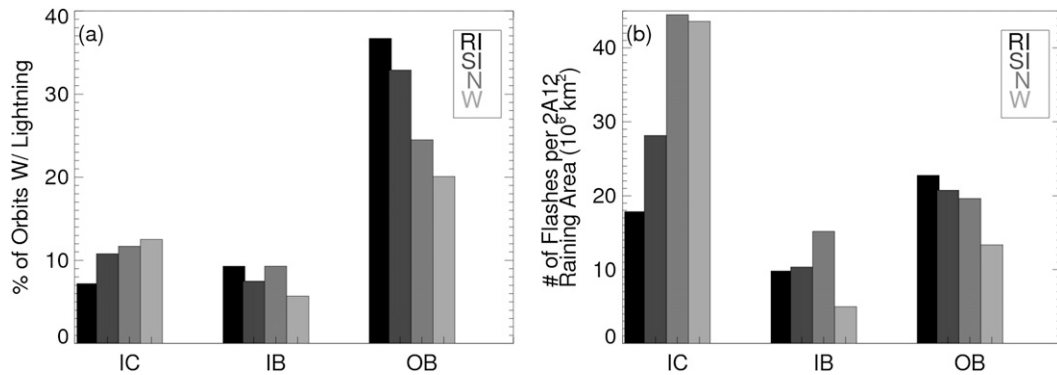


FIG. 7. Percentage of TC overpasses with (a) lightning and (b) flash count per 2A12 raining area in IC, IB, and OB regions of TCs in different intensity change stages.

rain, and convective intensity in the inner core is determined from the RI cases examined in this study. This is consistent with the well-agreed observation by TC forecasters and researchers that the storm must be well organized before intensifying and RI. As indicated by Figs. 2–6, the inner core region must be largely filled with at least moderate convection and moderate-to-heavy precipitation before RI. Some isolated asymmetric hot towers might exist and make contributions to the rapid intensification process in providing latent heating, but the necessary condition of RI is not those hot towers. As shown in Kieper and Jiang (2012), an early indicator of RI is the symmetric precipitative ring pattern around the storm center. Hot towers could be within the ring, but for about 50% of the RI cases, the ring, which occurs 24 h before RI, only contains shallow convection and warm rain. The findings in this study, along with those in Kieper and Jiang (2012), support a well-established theoretical result that the symmetric latent heating release is much more efficient for the vortex intensification than asymmetric heating (e.g., Nolan et al. 2007).

Results in section 3c (Fig. 7) are consistent with DeMaria et al. (2012), who showed that lightning density in the inner core of rapidly weakening storms is larger than that of RI storms, and the lightning density in the rainband regions is higher for RI storms. DeMaria et al. (2012) tried to explain this behavior using the different interaction of inner core and rainband with the environmental shear. Our results in sections 3a and 3b may help explain this from a different perspective. As shown above, the necessary condition for RI includes only moderate convective intensity and moderate-to-heavy rainfall in the inner core. To increase the likelihood of lightning, a fairly intense updraft is necessary to loft liquid droplets into the mixed phase region and to provide the supply of liquid hydrometeors, ice crystals,

and graupel (Rakov and Uman 2003; Saunders 2008). The inner core region in RI storms is therefore not optimal to produce lightning. As hypothesized by DeMaria et al. (2012), the interaction of the environmental shear with the inner core potential vorticity (PV) is largely responsible for the relationships between TC intensity changes and lightning density. The environmental vertical shear can tilt the inner core PV and induce asymmetric intense convection, which is favorable for both lightning and short-term storm intensification. However, the negative effects of the vertical shear, and sometimes the downdrafts and cold pools from the enhanced convection, halt the short-term intensification.

On the other hand, the outer rainband region is outside the core of high PV. As indicated by previous studies (Molinari et al. 1994; Houze 2010; DeMaria et al. 2012; JRC), the outer rainband region is similar to the background environment. The lightning density in that region is simply providing a measure of whether or not the storm environment is favorable for atmospheric convection. The result in Fig. 7 supports the notion that for RI storms, the environment is more favorable for outer rainband convection than that for non-RI storms.

## 5. Conclusions

Using 11-yr TRMM passive microwave radiometer, infrared, radar, and lightning data, this study has statistically quantified the rainfall and convective properties of tropical cyclones for different storm intensity change categories. Four 24-h future intensity change categories are defined as rapidly intensifying, slowly intensifying, neutral, and weakening. The storm inner core, inner rainband, and outer rainband regions were separated manually based on convective structures by a previous work presented in JRC.

It is found that at a weaker convective spectrum, RI storms have stronger ice scattering signature, higher cold cloud top, stronger radar reflectivity profile, and greater conditionally mean rain rate in the inner core than non-RI storms. However, at a stronger convective spectrum, the convective intensity in the inner core of RI storms is not stronger than that of non-RI storms. Instead, the inner core of RI storms has the lowest conditionally mean rain rate in the higher rain-rate spectrum (Figs. 2c,f) and the smallest near-surface radar reflectivity at the 90% percentile of the radar reflectivity profile (Fig. 5). The most important finding of this study is that RI storms always have larger raining area and total volumetric rain in the inner core.

All of these findings indicate that the maximum convective intensity in the inner core is not necessarily more intense prior to undergoing an RI episode than a slowly intensifying, neutral, or weakening episode. Instead, a minimum threshold of raining area, total volumetric rain, and convective intensity in the inner core has to be reached before a storm undergoes RI, at least for all the RI examples in the database used in this study. The following necessary conditions of inner rainfall and convective properties are found for RI: total raining area  $> 3000 \text{ km}^2$ , total volumetric rain  $> 5000 \text{ mm h}^{-1} \text{ km}^2$ , maximum near-surface radar reflectivity  $> 40 \text{ dBZ}$ , maximum 20-dBZ (40 dBZ) echo height  $> 8$  (4) km, minimum 85-GHz PCT  $< 235 \text{ K}$ , and minimum IR  $T_{\text{B11}} < 220 \text{ K}$ . These minimum values represent moderate-to-heavy rainfall and moderate convection in the inner core and are not commonly seen for all TCs. Therefore, the predictive power of these necessary conditions is that they will provide a simple and useful tool for forecasters to rule out RI. This tool is directly applicable to radar and satellite observations.

Above results are consistent with Jiang (2012), who demonstrated that extremely intense convection (i.e., hot towers) in the inner core increases the chance of RI, but the increase is not substantial. Similar to Kieper and Jiang (2012), this study supports the symmetric intensification mechanism proposed by previous studies, which showed that the axisymmetric latent heating release is more crucial for the vortex intensification than asymmetric heating (Ooyama 1969; Smith 1981; Shapiro and Willoughby 1982; Nolan et al. 2007).

The lightning analysis in this study has shown that the percentage of TRMM TC observations with lightning in the inner core decreases as the rate of storm intensification increases. The percentage is the lowest for storms that will undergo RI and the highest for weakening storms. However, for the outer rainband region, the reverse relationship is seen. The percentage of overpasses with lightning in the outer rainband region

is the highest for RI storms (37%), followed by storms in slowly intensifying (33%), neutral (25%), and weakening (20%) categories. The lightning density (per unit raining area) shows a similar relationship to the storm intensification. Overall, total lightning activities in the inner core (outer rainband) have a negative (positive) relationship with storm intensification. This is consistent with DeMaria et al. (2012), who used an independent lightning dataset and showed similar relationships.

This study treats all the global TCs together. The quality of best-track data is different for different TC basins. The quality of the North Atlantic best-track data is much higher than many of the other basins because of routine aircraft reconnaissance. Therefore, the best-track quality could be a factor causing uncertainty in the results. The preferred method is to treat each basin separately. Unfortunately, since RI is a rare event, there are not enough samples from TRMM to generate statistically significant results for individual basins yet.

*Acknowledgments.* Thanks are given to Drs. Ed Zipser, Dan Cecil, and Steve Krueger for useful comments on this research and to Dr. Chuntao Liu for assistance with the TRMM PF database. The authors also give acknowledgments to three anonymous reviewers, whose comments helped improve the manuscript substantially. Support for this study is provided by the NASA Precipitation Measurement Mission (PMM) Grant (NNX10AE28G), NASA New Investigator Program (NIP) Grant (NNX10AG55G), and NASA Hurricane Science Research Program (HSRP) Grant (NNX10AG34G). The authors thank Ramesh Kakar and Ming-Ying Wei (NASA headquarters) for their continued support of TRMM–PMM and hurricane sciences.

## REFERENCES

- Bell, M. M., and M. T. Montgomery, 2010: Sheared deep vertical convection in pre-depression Hagupit during TCS08. *Geophys. Res. Lett.*, **37**, L06802, doi:10.1029/2009GL042313.
- Cecil, D. J., and E. J. Zipser, 1999: Relationships between tropical cyclone intensity and satellite-based indicators of inner core convection: 85-GHz ice-scattering signature and lightning. *Mon. Wea. Rev.*, **127**, 103–123.
- , —, and S. W. Nesbitt, 2002: Reflectivity, ice scattering, and lightning characteristics of hurricane eyewalls and rainbands. Part I: Quantitative description. *Mon. Wea. Rev.*, **130**, 769–784.
- DeMaria, M., R. DeMaria, J. Knaff, and D. Molenaar, 2012: Tropical cyclone lightning and rapid intensity change. *Mon. Wea. Rev.*, **140**, 1828–1842.
- Gottelman, A., M. L. Salby, and F. Sassi, 2002: Distribution and influence of convection in the tropical tropopause region. *J. Geophys. Res.*, **107**, 4080, doi:10.1029/2001JD001048.
- Hall, T. J., and T. H. Vonder Haar, 1999: The diurnal cycle of west Pacific deep convection and its relation to the special and

- temporal variations of tropical MCSs. *J. Atmos. Sci.*, **56**, 3401–3415.
- Hendricks, E. A., 2012: Internal dynamical control on tropical cyclone intensity variability. *Trop. Cyclone Res. Rev.*, **1**, 97–105.
- , M. T. Montgomery, and C. A. Davis, 2004: The role of “vortical” hot towers in the formation of tropical cyclone Diana (1984). *J. Atmos. Sci.*, **61**, 1209–1232.
- , M. S. Peng, B. Fu, and T. Li, 2010: Quantifying environmental control on tropical cyclone intensity change. *Mon. Wea. Rev.*, **138**, 3243–3271.
- Houze, R. A., Jr., 2010: Clouds in tropical cyclones. *Mon. Wea. Rev.*, **138**, 293–344.
- , W.-C. Lee, and M. M. Bell, 2009: Convective contribution to the genesis of Hurricane Ophelia (2005). *Mon. Wea. Rev.*, **137**, 2778–2800.
- Iguchi, T., T. Kozu, R. Meneghini, J. Awaka, and K. Okamoto, 2000: Rain-profiling algorithm for the TRMM precipitation radar. *J. Appl. Meteor.*, **39**, 2038–2052.
- Jiang, H., 2012: The relationship between tropical cyclone rapid intensification and the strength of its convective precipitation features. *Mon. Wea. Rev.*, **140**, 1164–1176.
- , C. Liu, and E. J. Zipser, 2011: A TRMM-based tropical cyclone cloud and precipitation feature database. *J. Appl. Meteor. Climatol.*, **50**, 1255–1274.
- , E. M. Ramirez, and D. J. Cecil, 2013: Convective and rainfall properties of tropical cyclone inner cores and rainbands from 11 years of TRMM data. *Mon. Wea. Rev.*, **141**, 431–450.
- Kaplan, J., M. DeMaria, and J. A. Knaff, 2010: A revised tropical cyclone rapid intensification index for the Atlantic and eastern North Pacific basins. *Wea. Forecasting*, **25**, 220–241.
- Kelley, O. A., J. Stout, and J. B. Halverson, 2004: Tall precipitation cells in tropical cyclones eyewalls are associated with tropical cyclone intensification. *Geophys. Res. Lett.*, **31**, L24112, doi:10.1029/2004GL021616.
- , —, and —, 2005: Hurricane intensification detected by continuously monitoring tall precipitation in the eyewall. *Geophys. Res. Lett.*, **32**, L20819, doi:10.1029/2005GL023583.
- Kieper, M. E., and H. Jiang, 2012: Predicting tropical cyclone rapid intensification using the 37 GHz ring pattern identified from passive microwave measurements. *Geophys. Res. Lett.*, **39**, L13804, doi:10.1029/2012GL052115.
- Kummerow, C., W. S. Olson, and L. Giglio, 1996: A simplified scheme for obtaining precipitation and vertical hydrometeor profiles from passive microwave sensors. *IEEE Trans. Geosci. Remote Sens.*, **34**, 1213–1232.
- Lyons, W. A., and C. S. Keen, 1994: Observations of lightning in convective supercells within tropical storms and hurricanes. *Mon. Wea. Rev.*, **122**, 1897–1916.
- Machado, L. A. T., W. B. Rossow, R. L. Guedes, and A. W. Walker, 1998: Life cycle variations of mesoscale convective systems over the Americas. *Mon. Wea. Rev.*, **126**, 1630–1654.
- Mapes, B. E., and R. A. Houze, 1993: Cloud clusters and superclusters over the oceanic warm pool. *Mon. Wea. Rev.*, **121**, 1398–1416.
- McGaughey, G., E. J. Zipser, R. W. Spencer, and R. E. Hood, 1996: High resolution passive microwave observations of convective systems over the tropical Pacific Ocean. *J. Appl. Meteor.*, **35**, 1921–1947.
- Merrill, R. T., 1988: Environmental influences on hurricane intensification. *J. Atmos. Sci.*, **45**, 1678–1687.
- Mohr, K. I., and E. J. Zipser, 1996a: Defining mesoscale convective systems by their 85-GHz ice scattering signatures. *Bull. Amer. Meteor. Soc.*, **77**, 1179–1189.
- , and —, 1996b: Mesoscale convective systems defined by their 85-GHz ice scattering signature: Size and intensity comparison over tropical oceans and continents. *Mon. Wea. Rev.*, **124**, 2417–2437.
- Molinari, J., P. K. Moore, V. P. Idone, R. W. Henderson, and A. B. Saljoughy, 1994: Cloud-to-ground lightning in Hurricane Andrew. *J. Geophys. Res.*, **99** (D8), 16 665–16 676.
- , —, and —, 1999: Convective structure of hurricanes as revealed by lightning locations. *Mon. Wea. Rev.*, **127**, 520–534.
- Montgomery, M. T., and R. K. Smith, 2011: Paradigms for tropical-cyclone intensification. *Quart. J. Roy. Meteor. Soc.*, **137**, 1–31.
- , M. E. Nicholls, T. A. Cram, and A. B. Saunders, 2006: A vortical hot tower route to tropical cyclogenesis. *J. Atmos. Sci.*, **63**, 355–386.
- Nguyen, S. V., R. K. Smith, and M. T. Montgomery, 2008: Tropical cyclone intensification and predictability in three dimensions. *Quart. J. Roy. Meteor. Soc.*, **134**, 563–582.
- Nolan, D. S., and L. D. Grasso, 2003: Nonhydrostatic, three-dimensional perturbations to balanced, hurricane-like vortices. Part II: Symmetric response and nonlinear simulations. *J. Atmos. Sci.*, **60**, 2717–2745.
- , Y. Moon, and D. P. Stern, 2007: Tropical cyclone intensification from asymmetric convection: Energetics and efficiency. *J. Atmos. Sci.*, **64**, 3377–3405.
- Ooyama, K., 1969: Numerical simulation of the life cycle of tropical cyclones. *J. Atmos. Sci.*, **26**, 3–40.
- Rakov, V. A., and M. A. Uman, 2003: *Lightning: Physics and Effects*. Cambridge University Press, 687 pp.
- Rao, G. V., and P. D. MacArthur, 1994: The SSM/I estimated rainfall amounts of tropical cyclones and their potential in predicting the cyclone intensity changes. *Mon. Wea. Rev.*, **122**, 1568–1574.
- Reasor, P. D., M. T. Montgomery, and L. Bosart, 2005: Mesoscale observations of the genesis of Hurricane Dolly (1996). *J. Atmos. Sci.*, **62**, 3151–3171.
- Saunders, C., 2008: Charge separation mechanisms in clouds. *Space Sci. Rev.*, **137**, 335–353.
- Shapiro, L. J., and H. E. Willoughby, 1982: The response of balanced hurricanes to local sources of heat and momentum. *J. Atmos. Sci.*, **39**, 378–394.
- Sippel, J. A., J. W. Nielsen-Gammon, and A. E. Allen, 2006: The multiple vortex nature of tropical cyclogenesis. *Mon. Wea. Rev.*, **134**, 1796–1814.
- Smith, R. K., 1981: The cyclostrophic adjustment of vortices with application to tropical cyclone modification. *J. Atmos. Sci.*, **38**, 2021–2030.
- Spencer, R. W., H. M. Goodman, and R. E. Hood, 1989: Precipitation retrieval over land and ocean with the SSM/I: Identification and characteristics of the scattering signal. *J. Atmos. Oceanic Technol.*, **6**, 254–273.
- Steranka, J., E. B. Rodgers, and R. C. Gentry, 1986: The relationship between satellite measured convective bursts and tropical cyclone intensification. *Mon. Wea. Rev.*, **114**, 1539–1546.
- Yuter, S. E., and R. A. Houze, 1995: Three-dimensional kinematic and microphysical evolution of Florida cumulonimbus. Part II: Frequency distributions of vertical velocity, reflectivity, and differential reflectivity. *Mon. Wea. Rev.*, **123**, 1941–1963.
- Zuidema, P., 2003: Convective clouds over the Bay of Bengal. *Mon. Wea. Rev.*, **131**, 780–798.